Manipulation of Electromagnetic Waves Based on New Unique Metamaterials: Theory & Applications

Q. Wu, K. Zhang, and G. H. Yang

Department of Microwave Engineering
Harbin Institute of Technology, Harbin, 150001, China
qwu@hit.edu.cn, zhangkuang@hit.edu.cn, gh.yang@hit.edu.cn

Abstract ─ Metamaterials are typically engineered by arranging a set of unit cells in a regular array throughout a region of space, thus, obtaining some desirable macroscopic electromagnetic behavior. The desired property is often one that is not normally found naturally (negative refractive index, near-zero index, etc.). Over the past few years, the flexibilities of the metamaterials in choosing the numerical value of the effective permittivity or permeability have led to kinds of novel theoretical and practical possibilities for different applications, ranging from microwave to optical regime. In this paper, the theoretical mechanism for constructing metamaterials is described, and the unique feature of electromagnetic waves can be manipulated is verified by their applicability to construct various devices or components Some typical application is given, including: (1) novel RF devices realized by optical transformation principle, such as energy concentrators and universal waveguide connectors; (2) metamaterial-based wave absorbers; (3) gain enhancement approach of aperture antennas by planar metamaterial lenses loaded; (4) ultra-thin lenses with dual-polarization filtering features; and (5) beam tunable antennas by metamaterial device. Undoubtely, the reported results suggest promising applications in the next-generation communication system.

Index Terms ─ Absorbers, antennas, lenses, metamaterials.

I. INTRODUCTION

Recently, metamaterials have been attracting growing attentions. Responding to the incident electric and/or magnetic fields, metamaterials could exhibit specific effective permittivity ε and/or permeability μ, including the Double Negative (DNG for short, the real part of both ε and μ is negative, which was first proposed by Veselago theoretically in 1968 [1]), Single Negative (ENG [2] or MNG [3] for short, the real part of ε or μ is negative), and the Zero-Index Metamaterials [4] (ZIM, the real part of ε and/or μ is near zero). Due to the exotic electromagnetic characteristics, metamaterials have shown great potentials in kinds of applications, such as invisibility cloak [5], perfect lens [6], and many other kinds of novel applications in microwave [7-9], terahertz [10] and optical regime [11], etc.

Manipulation of electromagnetic waves as desired has been a hot topic in the field of electromagnetism for a long time. The emerge of metamaterials provides great opportunity for the control of the transmissions and distributions of electromagnetic waves and energy. In this paper, the applications of metamaterials in the manipulation of electromagnetic waves are discussed. In Section II, the theory of transform optics is introduced. Then based on the form invariance's properties, electromagnetic energy concentrator and waveguide connector are proposed and simulated. After simplification processing of constitution parameters, the proof-of-principle experiment is completed to verify the theoretical work. In Section III, metamaterials are applied to build a novel broadband absorber. In Section IV, zero index metamaterials with matched impedance are constructed and applied to enhance the gain of horn antenna. Measurements of gain and far-field pattern verify the theoretical design. In Section V, ultra-thin lens is proposed based on the phase discontinuities. Due to the

Submitted On: March 1, 2014
Accepted On: August 8, 2014

different response to the helicity of the incidence, dual-polarization ultra-thin lens is proposed and simulated. Simulations show good agreement with theoretical results. In Section VI, a novel method of building electronically beam steerable antenna system using Active Frequency Selective Surfaces (AFSS) is proposed. The design methods and special principals of the active frequency selective surfaces built for flexible antenna beam scanning are studied. The antenna system is fabricated and experimentally investigated. The front-to-back ratio is more than 30 dB with the null point of -59 dB. The gain can be promoted to be 7.0 dBi. Furthermore, multi-beam functionality is achieved and the amplitudes of the beams can be controlled. It is believed, that all these studies suggest potential applications in the communication system or subsystems.

II. THEORY OF TRANSFORM OPTICS AND APPLICATIONS

The transform optics was first proposed based on the remarkable fact that Maxwell's equations are form-invariant under any coordinate transformation. Maxwell's equations still preserve their form inside the transformed space, but the material transforms into an anisotropic material to convey the effect of the coordinate transformation to the electromagnetic fields. This feature provides an intuitive way of designing material tuning the electromagnetic fields in a desired manner, which has led to numerous useful and beautiful applications. The transform optics has also started a new era for design and application of metamaterials in the manipulation of electromagnetic waves.

A. Transform optics description

Suppose a general transformation f transform the original space α to the transformed space α', which also map each point P in the original space into P' in the transformed space. In order to preserve the form invariance of Maxwell's equations, the general transformation yields an inhomogeneous and anisotropic material. The constitutive parameters can be then derived as:

$$\overline{\overline{\varepsilon}}' = \frac{JJ^T}{\det(J)}\overline{\overline{\varepsilon}}, \tag{1a}$$

$$\overline{\overline{\mu}}' = \frac{JJ^T}{\det(J)}\overline{\overline{\mu}}, \tag{1b}$$

where J is the jacobian transform matrix defined as:

$$J = \begin{bmatrix} \frac{\partial x'}{\partial x} & \frac{\partial x'}{\partial y} & \frac{\partial x'}{\partial z} \\ \frac{\partial y'}{\partial x} & \frac{\partial y'}{\partial y} & \frac{\partial y'}{\partial z} \\ \frac{\partial z'}{\partial x} & \frac{\partial z'}{\partial y} & \frac{\partial z'}{\partial z} \end{bmatrix}, \tag{2}$$

in the Cartesian coordinates. Then according to equation (1)-(2), the constitutive parameters of the transformed material can be calculated according to certain function of transformation. Here, below we will use the transform optics to achieve the polygonal cloak, electromagnetic energy concentrator and the waveguide connector.

B. Realization of the transform optics

First, the cylindrical EM concentrator is taken into consideration. The optical transformation for the concentrator can be expressed that the region $r'\in[0, R_2]$ is compressed into the region $r\in[0, R_1]$, and the region $r'\in[R_2, R_3]$ is stressed into the region $r\in[R_1, R_3]$, as shown in Fig. 1. Here, r and r' represents the radius of the physical space and the virtual space, respectively. For the transformation between $r'\in[0, R_2]$ and $r\in[0, R_1]$, namely the core region, the transformation function can be easily expressed as the linear function. For the circular region, the numerical value of ε_r and ε_θ is reciprocal, if one of them is set as a constant, the other can be also fixed as constant. Based on this relationship we can establish the ordinary differential equation, and the solution is the constitutive tensor for the circular region, which can be expressed as:

$$\varepsilon_\theta = \frac{1}{\varepsilon_r} = m_0, \tag{3a}$$

$$\varepsilon_z = m_0\left(\frac{r}{R_3}\right)^{2(m_0-1)}, \tag{3b}$$

where $m_0 = \log_{\frac{R_3}{R_1}}\frac{R_3}{R_2}$. Hence, we have obtained all the constitutive parameters of the cylindrical EM concentrator. It could be seen that the relative permittivity ε_r and ε_θ are obtained as constants, and only ε_z is the function of radius, which could also be homogenized through layered structure.

Furthermore, it can be observed in equation (3) that the constitutive tensor is nonsingular and positive, which improves the flexibilities for 2D EM concentrator design. Moreover, the impedance of the concentrator at the outer boundary can be expressed as $Z\big|_{r=R_3}=\sqrt{\mu_\theta/\varepsilon_z}=1$. The EM concentrator is always impedance matched with the free space, which indicates minimized scattering fields of the concentrator.

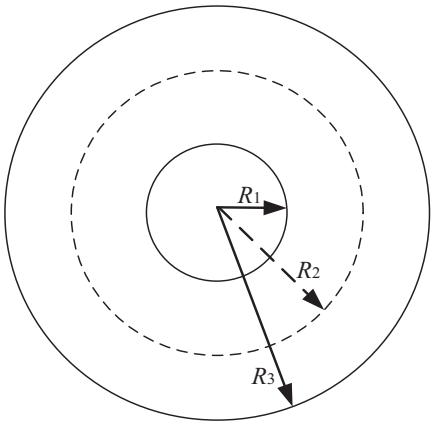

Fig. 1 Sketch of the cylindrical EM concentrator.

Then lossless cases are studied based on the simulation results of the commercial software based on Finite-Element Method (FEM). Here, the geometry parameters are selected that $R_3=2R_2=4R_1=0.4$ m, and the frequency is selected at 2 GHz. Based on all the geometry parameters, the constitutive parameters of the circular region can be calculated through equation (3). Figure 2 (a) shows the electric fields distributions of the concentrator. It can be seen that the electric fields are concentrated into the inner core region smoothly, and the fields outside are rarely disturbed. Furthermore, the power flow of the EM fields are also calculated and shown in Fig. 2 (b). It can be seen that power flow is enhanced obviously in the inner core region. Through the transformation function of equation, it can be observed that the enhancing ratio can be expressed as the ratio of R_2 and R_1, and enhancement theoretically diverges to infinity as R_1 goes to zero [11]. It should be noted that in our design, all components but one in the constitutive tensor are constants. Compared with the former results [5], our design provides greatly facility for the practical constructions.

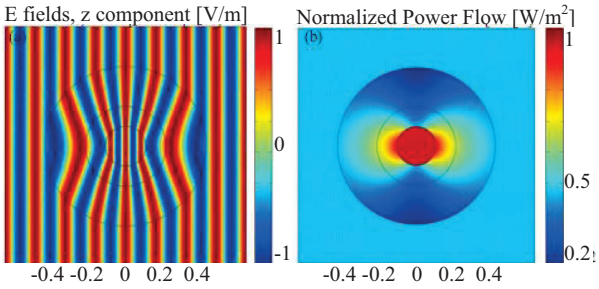

Fig. 2. (a) Electric field distributions of the cylindrical EM concentrator, and (b) normalized power flow distribution of the concentrator.

Second, we focus our concentration on the waveguide connector shown in Fig. 3 (a). Here, finite embedded optical transformation is applied to the design of waveguide connector. Considering a Two-Dimensional (2D) structure in the Cartesian coordinate system, the optical transformation that transfers the original space ABCD into the transformed space ABC'D', can be simply defined as the linear function. Then, the constitutive parameters can be derived according to equation (1) and (2). For the facility of the construction of the connector, here, we just consider the Transverse Magnetic (TM) polarization, for which only ε_{xx}, $\varepsilon_{xy}(\varepsilon_{yx})$, ε_{yy} and μ_{zz} components of the constitutive tensor are relevant. Furthermore, the nonmagnetic material parameters can be transformed into the diagonal matrix through rotating its optical axis by a certain angle with the z-axis, as shown in Fig. 3 (b). Moreover, the anisotropic metamaterial with diagonal constitutive tensor can be expressed by the two alternating mediums based on the effective medium theory.

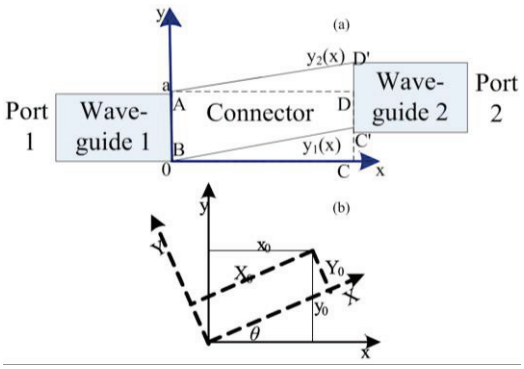

Fig. 3. (a) Sketch of the waveguide connector, and (b) sketch of the rotated coordinate.

In order to support the theoretical results, a proof-of-concept experiment is conducted in the microwave frequency. The system above is designed and fabricated, including the following parts: two square waveguides (40mm*40mm*100mm, as shown in Fig. 4 (a)), two coaxial-to-waveguide adapters (inner radius of the cylindrical cavity is 3.25 mm and 17 mm respectively, and the length of each cavity is 12.5 mm, as shown in Fig. 4 (b)) and the connector (40mm*40mm*50mm, as shown in Fig. 4 (c)) with the slope of 16.7°. For the alternating dielectric materials filled in the connector, the microwave composite-dielectric substrate and air are selected, whose relative permittivity is 5.5 and 1, respectively. To satisfy the effective medium theory, the thickness of the microwave composite substrate and the air spacing is set as 1.5 mm and 3 mm (about 0.03λ and 0.06λ with respect to the central working frequency, as shown in Fig. 4 (d), respectively.

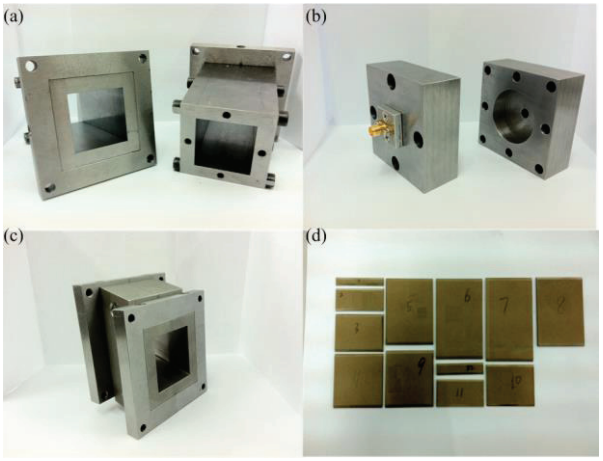

Fig. 4. The photos of the fabricated proof-of-concept experimental system, including: (a) the square waveguides, (b) the coaxial-to-waveguide adapters, (c) the connector, and (d) the dielectric slabs.

Then, the transmission parameters (S_{21}) of three cases are tested around 6 GHz through the vector network analyzer (Agilent E8363B): (I) the single square waveguide; (II) the connector filled with only air; and (III) the connector filled with alternating dielectric slabs. Here, all the other experimental data are normalized by the experimental result of the S_{21} of the single square waveguide (case (I)), and the experimental results are shown in Fig. 5. It could be seen that when filled with the material with designed constitutive parameters and geometrical parameters, the connector can achieve the relative high transmission parameters around the central working frequency, compared to the connector filled just with air. So the design principles and the constitutive parameters proposed are verified [7].

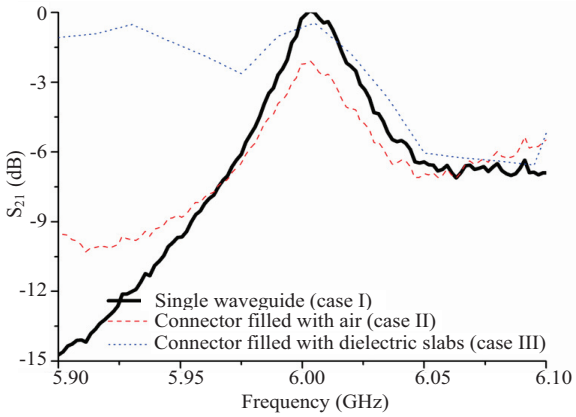

Fig. 5. The experimental results of the transmission parameters (S_{21}).

III. BROADBAND POLARIZATION-INSENSITIVE ABSORBER BASED ON METAMATERIALS

A. Gradient structure absorber

A gradient structure absorber is presented in this section. The unit cell geometry of the proposed Metamaterial Absorber (MA) is illustrated in Fig. 6. The top layer consists of gradient Split Resonant Rings (SRRs), Square Metallic Patches (SMPs) and resistors mounted crosswire. The lossy dielectric board and the bottom layer is same as the single SRR absorber. Side length of dielectric substrate unit cell is A=29.6 mm, while thickness is D=1.6 mm. Length of crosswire is c=7 mm. The split width of SRRs and separation distance between adjacent crosswire is g=0.4 mm. Width of all copper wire is w=0.6 mm. Resistance value is R=50 Ω. The side length of gradient SRRs and SMPs are aij and bij respectively, which is given in Table 1.

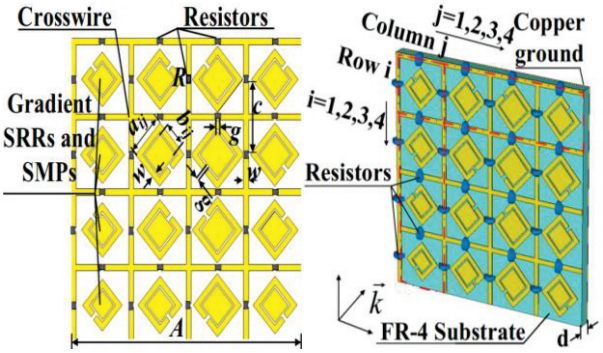

(a) The plan view (b) The stereogram

Fig. 6. The structure of the unit cell of the proposed MA.

Table 1: The sizes of gradient of SRRs and SMPs

a_{ij}, b_{ij}/mm	j=1	j=2	j=3	j=4
i=1	3.8, 2.2	4.2, 2.6	4.6, 3.0	4.2, 2.6
i=2	4.0, 2.4	4.4, 2.8	4.8, 3.2	4.4, 2.8
i=3	3.8, 2.2	4.2, 2.6	4.6, 3.0	4.2, 2.6
i□□	3.6, 2.0	4.0, 2.4□	4.4, 2.8	4.0, 2.4

Every four SRRs and SMPs are put obliquely around the central crosswire. There are 16 pairs of SRRs and SMPs in each unit cell, which are designed with gradient length parameters to make the 16 pairs resonator resonant at adjacent frequencies to increase the operating frequency band. In addition, the resistors mounted crosswire is leaded in this structure which is able to draw into a new resonant frequency to further increase the bandwidth. Moreover, resistors could transfer EM energy to heat and fulfill resistive loss through which the quality factor of the MA is decreased and the bandwidth is increased. Through simulation and optimization, resistance R=50 Ω is selected. It is worth mentioning that the structures of the unit cell are all almost symmetry so that the MA will have similar absorption effect on both TE and TM wave; namely, the MA should be polarization-insensitive.

The unit cell is simulated in CST MWS 2012 with PBC. In order to illustrate the absorbing mechanism of the proposed MA, two cases at 16.48 GHz and 24.64 GHz are selected as examples. The magnetic field distribution and surface currents at the two frequencies for TE wave are illustrated in Fig. 7. It can be summarized from Fig. 7, that the strong absorption of broadband EM wave is based on the two following points: firstly, it can be observed that a strong magnetic field is generated around the SRR and SMP which form the "magnetic loop trap" structure. The EM energy is stored around this structure, which effectively blocks the EM wave to spread outwards. Thus, current is excited on the top of the unit cell. In this way, EM wave could be consumed in the FR-4 dielectric substrates and the chip resistors. Secondly, comparing with the surface current distribution at two different frequencies, it can be seen clearly that different SRRs of the unit cell resonate at corresponding frequencies. Since the presence of the gradient structure, the unit cell contains resonators at adjacent frequencies which make the absorber function in a broadband frequency.

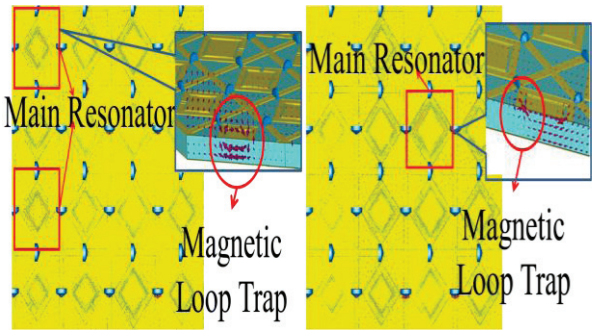

(a) 16.48 GHz (b) 24.64 GHz

Fig. 7. The simulated surface current and magnetic field distribution.

It can be observed from Fig. 8, that S_{11} is quite small in a wide band and S_{21}=0 as expect. From Fig. 9, it can be obtained that for both TE and TM waves, the absorption rate of the absorber are both larger than 60% from 12.38 GHz to 22.28 GHz, whose relative bandwidth is 57.13%. The maximum absorption rate of the MA is 98.37% in this frequency band. In addition, it is worth noting that the substrate used in this paper is ordinary FR-4 with a loss tangent of only 0.025. MA in use of higher-loss-tangent materials is expected to obtain a better absorption property.

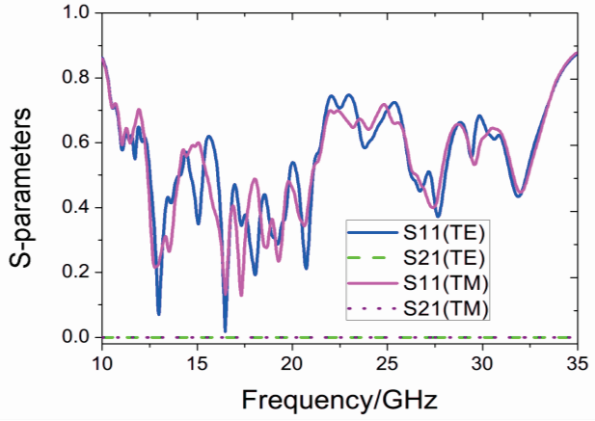

Fig. 8. The simulated S-parameters for TE wave and TM wave.

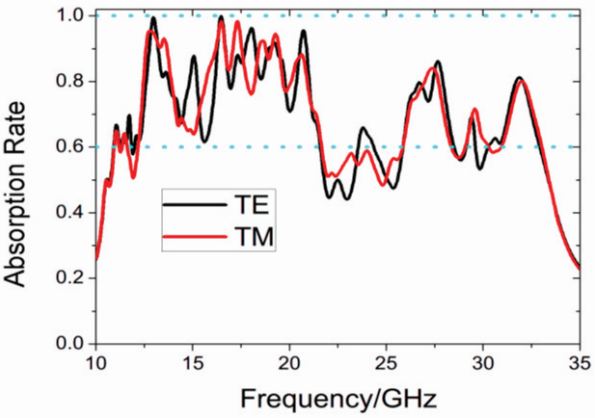

Fig. 9. The calculated absorption rate for both TE and TM wave.

IV. METAMATERIAL LENS-ELECTRIC AND MAGNETIC RESONANCE STRUCTURE

Zero Index Metamaterial (ZIM) has been investigated comprehensively for directive emission since 2002 [4]. Varieties of designs of ZIM have been presented to enhance antenna directivity and gain. However, the impedance match between ZIM and free space is always hard to achieve. The antenna and ZIM should be designed together and ZIM is not universal for different kinds of antennas. In this section, a Metamaterial Lens (ML) is presented for antenna directivity and gain enhancement.

A. The construction of the ZIM unit cell

The structure and the corresponding parameters are illustrated in Fig. 10. The magnetic resonant structure is Modified Split Ring Resonator (MSRR), which is composed of two square rings with two slot at the opposite sides. MSRR is introduced for its larger bandwidth. The metal patch in Fig. 10 is the electric resonant structure of the ZIM unit cell. The unit cell is simulated in CST MWS. Its *S*-parameters are depicted in Fig. 11 and a large passband centered at 9.9 GHz with high S_{21} is observed.

The constitutive parameter extracted from the S-parameters are calculated and depicted in Fig. 12, which is based on the algorithm of [12]. It can be seen that μ_{eff} and ε_{eff} in turn approach zero at 9.4 GHz and 9.7 GHz, respectively, which will make the corresponding effective refractive index n to be near zero in a band as broad as possible [13]. Particularly, at 9.0 GH and 9.9 GHz, one finds that the effective permittivity and permeability has the same value of 0.8 and 0.3, respectively, which leads the ZIM to have both near-zero refractive index for directive emission and perfectly wave impedance matching with free space.

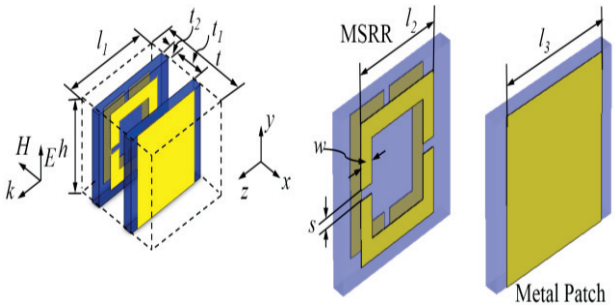

Fig. 10. The structure and parameters of the unit cell, in which l_1=8 mm, l_2=5.4 mm, l_3=h=6.6 mm, t=8.2 mm, t_1=2.9 mm, t_2=0.8 mm, w=0.8 mm and s=0.4 mm.

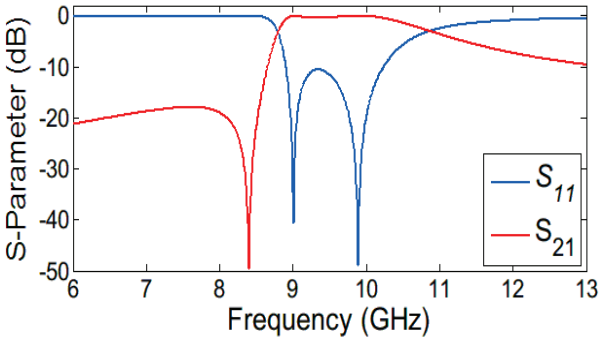

Fig. 11. The S-Parameters of the unit cell.

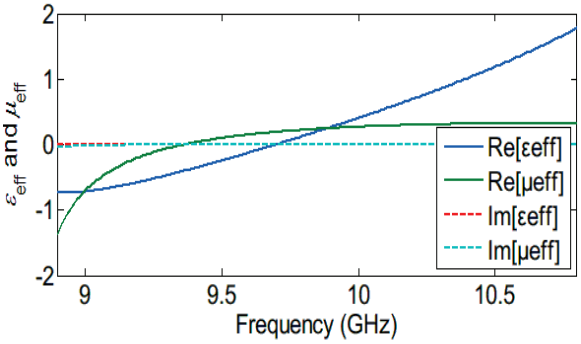

Fig. 12. The effective constitutive parameters of the unit cell.

B. Fabricated and tested planar metamaterial lens

The Metamaterial Lens (ML) is formed by arranging the unit cell in one plane. It is fabricated and measured with an H-plane horn antenna with center frequency of 9.9 GHz, as shown in Fig. 13.

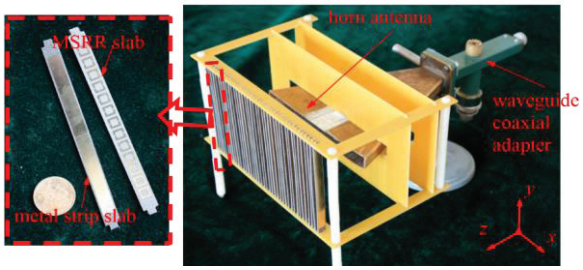

Fig. 13. The phototype of ML and the H-plane horn antenna.

For the H-plane horn antenna, the size of the ML is 19×13 unit cells. The measured return loss of the horn antenna is depicted in Fig. 14. The return loss of the H-plane horn antenna is also slightly affected by the ML. The measured E-plane radiation patterns of the H-plane horn antenna with and without ML are illustrated and contrasted in Fig. 15. The main lobe of the E-plane radiation pattern of the antenna at 9.9 GHz is obviously sharpened. The main lobe width is reduced from 91.4° to 14.8°. The directivity of the H-plane horn antenna is greatly enhanced. The antenna gain of the H-plane horn antenna is also enhanced by 4.43 dB, which is a significant improvement. The gain enhancement of the ML with different distance between the lens and antenna is also depicted in Fig. 16. The ML proposed in this section is capable of enhancing antenna gain in a wideband from 9.5 GHz to 10.6 GHz. Additionally, the gain enhancement barely varies with the distance thanks to good impedance match between lens and free space, which is an advantage over lens based on Fabry-Perot resonance [14].

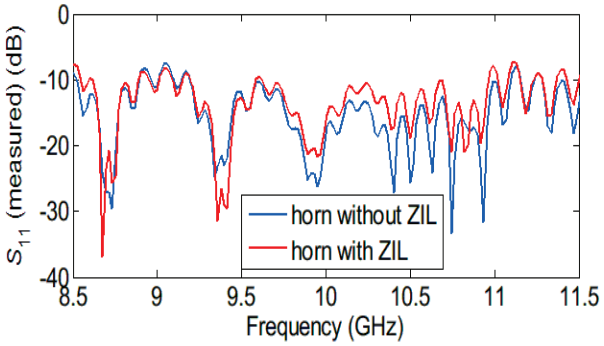

Fig. 14. The measured return loss of the H-plane horn antenna with and without the ML, here ZIL in the legend is short for zero-index lens.

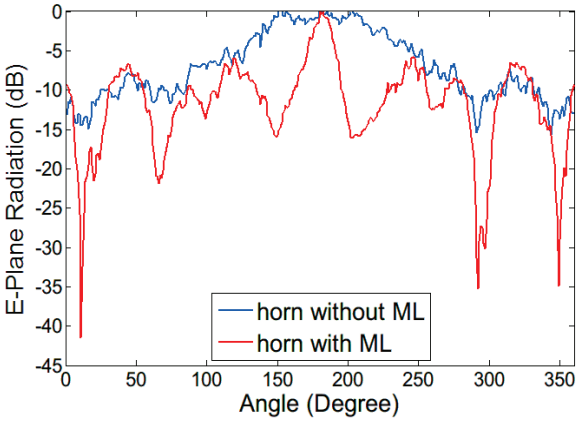

Fig. 15. The E-plane radiation pattern of the H-plane horn antenna with and without the ML.

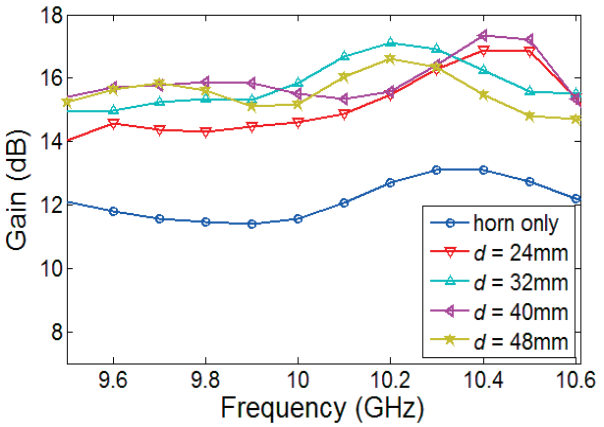

Fig. 16. The gain enhancement of the H-plane horn antenna loading ML with different distance.

V. ULTRA-THIN PLANAR METALENS WITH PHASE DISCONTINUITY

The metalens with phase discontinuity provides the abrupt phase change at the interface. By introducing abrupt phase changes with sub-wavelength unit cells, phase accumulation in the traditional lens can be substituted by the phase discontinuities on the interface, which provides possibilities of constructing the ultra-thin metalens. However, the conversion efficiency, defined as the ratio of the energy of transmitted cross-polarized wave to that of the total incident wave, is relatively low for the published designs operating under cross-polarized fields [15,16], and the maximum efficiency achieved was only a few percent. It was predicted theoretically, that the maximum attainable cross-coupling is 25%, based on the S-parameters of the four ports network [17].

A. Unit cell structure

The proposed metalens and the unit cell are schematically shown in Fig. 17 (a) and (b), respectively. The unit cell has a miniaturized structure, which is beneficial for more compact design. For the normal incident plane wave linearly polarized along x- or y-axis, the transmission coefficients are shown in Fig. 17 (c), while Fig. 17 (d) illustrates the transmission coefficients for the transmitted Left-Circularly Polarized (LCP) and Right-Circularly Polarized (RCP) components under LCP incident wave. Simulation results also show that the transmission coefficients are independent of θ, which depicts the orientation angle of the optical axes of the individual unit cell in clockwise direction with respect to y-axis, as shown in Fig. 17 (b).

To achieve the desired phase changes in microwave band, the P-B phase is adopted here. A Phase Factor (PF) is achieved when the polarization changes from the initial state to the final state. The two poles on the Poincaré sphere indicate the RCP and LCP states. The PF is equal to half of the area, which is encompassed by the loop on the sphere, and the absolute value can be calculated as $2|\theta_1-\theta_0|$. Using Jones calculus, the transmitted field of the P-B elements can be given by Eq. (4) as:

$$\left|\vec{E}_{out}\right\rangle = \sqrt{\eta_E}\left|\vec{E}_{in}\right\rangle + \left(\sqrt{\eta_R}e^{\pm i2\theta}\left|\vec{R}\right\rangle + \sqrt{\eta_L}e^{\mp i2\theta}\left|\vec{L}\right\rangle\right), \quad (4)$$

where $\eta_E = \left|\frac{1}{2}(t_x + t_y e^{i\phi})\right|^2$, $\eta_R = \left|\frac{1}{2}(t_x - t_y e^{i\phi})\left\langle\vec{E}_{in}\right|\vec{L}\right\rangle\right|^2$, $\eta_L = \left|\frac{1}{2}(t_x - t_y e^{i\phi})\left\langle\vec{E}_{in}\right|\vec{R}\right\rangle\right|^2$ and η_E, η_R, η_L are the polarization order coupling efficiencies, <|> denotes inner product, $\left|\vec{R}\right\rangle$ ($\left|\vec{L}\right\rangle$) represents the RCP (LCP) component, t_x and t_y are the amplitudes of the transmission coefficients for two linear polarizations which are perpendicular and parallel to the optical axes, and φ is the phase difference between the transmission coefficients.

When RCP (or LCP) is the incident wave, η_R (or η_L) equals to zero, and Eq. (4) illustrates that the transmitted field from a P-B element comprises two polarization orders. One maintains the phase and original polarization state of the incident wave, while the other one exhibits opposite helicity and a phase modification of ±2θ, where ±1 corresponds to both the rotating direction of the unit cells and the helicity of the incidence. Therefore, by arranging the unit cell with different orientations an ultra-thin metalens with the phase discontinuity can be achieved, and EM waves can be manipulated with great latitude subsequently.

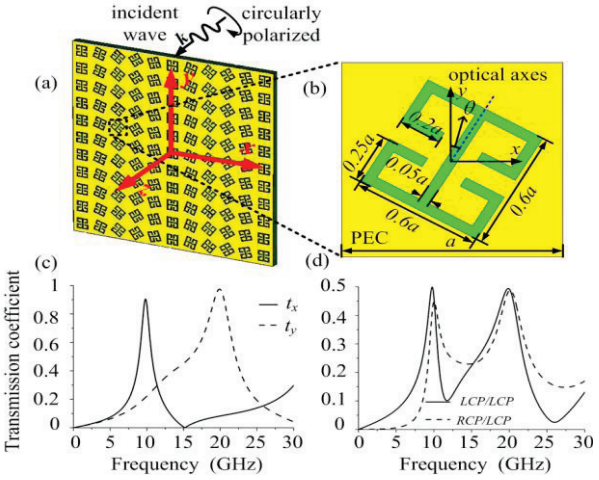

Fig. 17. Illustration of the transmission of EM waves through the unit cell: (a) sketch of the metalens, (b) geometric parameters of the unit cell, (c) transmission coefficients under linear-polarized incident wave when θ=0, and (d) transmission coefficients under LCP incident wave when θ=0.

In this research, we find that at the first resonant frequency of 9.8 GHz, the incident wave with linear polarization along x-axis can pass through the lens completely, while transmission is suppressed for y-polarized incidence, as shown in Fig. 17 (c). As a result, when the incident wave is circularly polarized, half of the incident energy can transmit. Figure 17 (d) shows that the cross-polarized and co-polarized fields both exist in the transmitted field under LCP incident wave. The transmission coefficients for the transmitted LCP and RCP components are the same with value 0.5 at the first resonance, which means that our design has reached the theoretical limit on the maximum coupling efficiency of 25% for cross-polarized component.

B. Bi-functional ultra-thin metalens design

As demonstrated above, the unit cell of metalens responds differently to the LCP and RCP incident wave. Thus, we can utilize this phenomenon to construct bi-functional metalens. For a given focal length f, Eq. (5) gives the relationship between the rotation angle θ and the position of the unit cells:

$$\theta = \pm 0.5 \frac{2\pi}{\lambda}(\sqrt{f^2 + x^2} - |f|), \qquad (5)$$

where x=na (n=0, ±1, ±52, …), and ±1 represents the clockwise or anti-clockwise rotation respectively. In this letter, a metalens with focal length *f* of 300 mm is proposed. The working frequency is around 10 GHz, thus, it can be considered to be operating in the far-field region (f ≈10λ). Figures 18 and 19 show the results of the electric field distribution. It can be seen that for the normal RCP incident wave, the design operates as an ultra-thin converging lens (Fig. 18 (a)). When the polarization of the incident plane wave changes into LCP, the metalens exhibits a diverging effect (Fig. 19 (a)). According to Eq. (4), the transmitted cross-polarized component is affected by the lens, and the transmitted co-polarized component keeps original state. Although, not as perfect as the pure cross-polarized transmission, the total fields still perform the same converging or diverging effects after superimposed with the transmitting co-polarized wave. This makes our metalenses competitive for practical applications. In general, our design can be tailored to be working as converging or diverging lens only depending on the helicity of the incident plane wave.

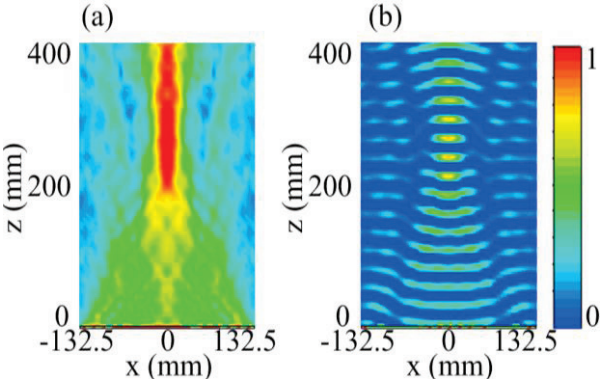

Fig. 18. (a) Simulation result of the distribution of the transmitted electric fields amplitude of pure cross-pol component for the converging lens, and (b) simulation result of the distribution of the transmitted E_y component.

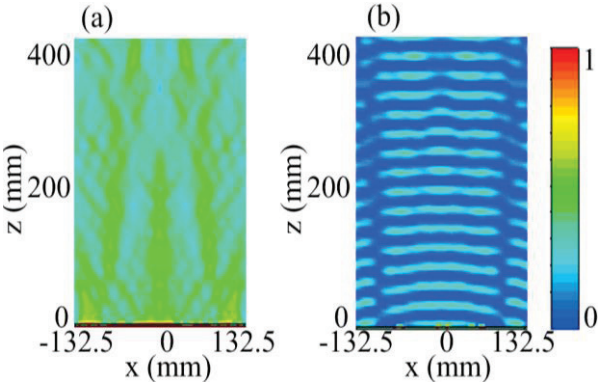

Fig. 19. (a) Simulation result of the distribution of the transmitted electric fields amplitude of pure cross-pol component for the diverging lens, and (b) simulation result of the distribution of the transmitted E_y component.

VI. ELECTRONICALLY RADIATION PATTERN STEERABLE ANTENNAS USING ACTIVE FREQUENCEY SELECTIVE SURFACES

With the expansion of wireless communication industry, the demand for electronically steerable antenna solutions is increasing such as point-to-multi-point links for base stations.

In this work, a new method to build 360° steerable antenna is proposed. The control

methods and design requirements for both single- and multi-beam modes are presented and discussed. The working mechanism is to modify the path of EM wave emitted from the inner antenna using AFSS mounted with varactor diodes. Another advantage of using varactor diodes is the low power consumption. Unlike the PIN diodes, when varactor diodes are reversely biased, the leakage current is low. In this work, the total power consumption is less than 1.02 mW.

A. Configuration and beam scanning

As shown in Fig. 20, ten columns of AFSS unit cells are employed to construct a cylinder array with a radius of 50 mm. Figure 21 shows three methods to configure the antenna in each sector for single-beam mode. Multi-beam ability is also studied in this work. With the help of continuously tuning capability, the amplitudes of the beams can be also controlled. Figure 22 illustrates two cases for introduction, there are many other combinations.

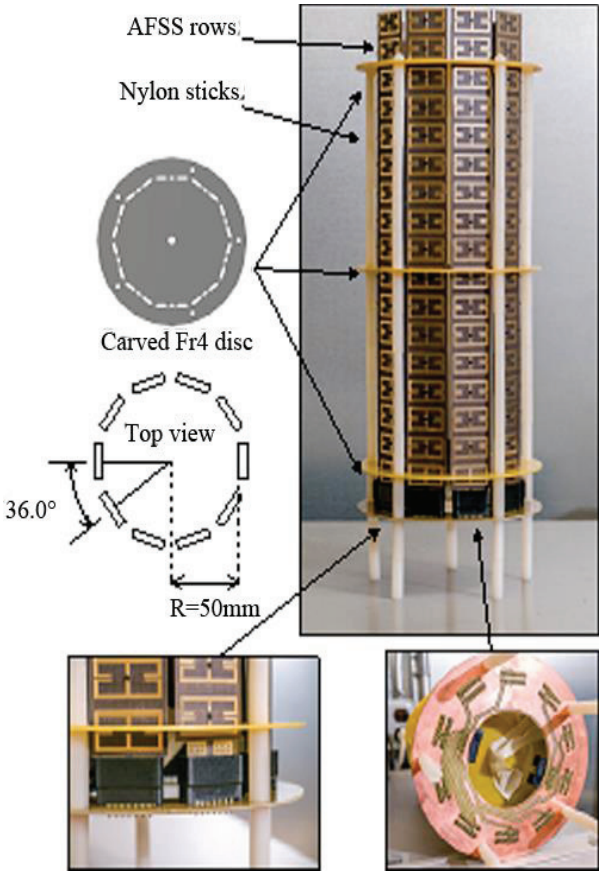

Fig. 20. Antenna structure and installation.

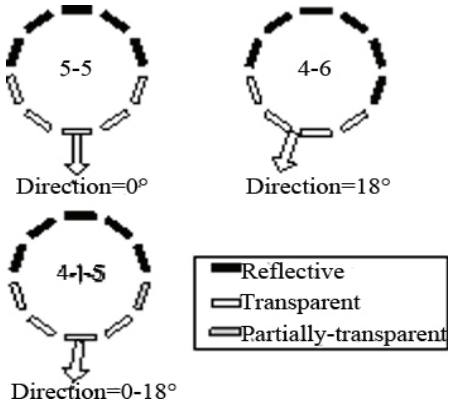

Fig. 21. Single-beam control methods.

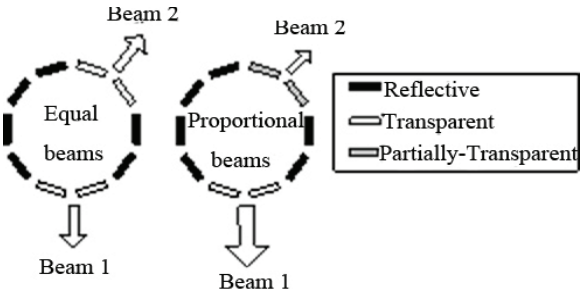

Fig. 22. Multi-beam control methods.

B. AFSS array

The structure of AFSS unit is shown in Fig. 23. The top side of the unit cell consists of a pair of vertical-symmetric anchor-shaped metal strips and a varactor mounted in the middle. The bottom side includes the DC biasing network, as shown in the bottom view in Fig. 23.

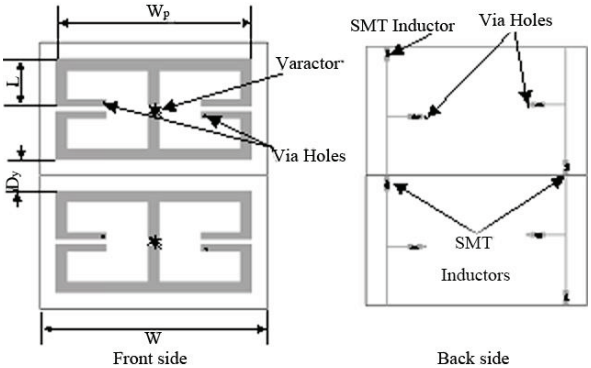

Fig. 23. Layout of the unit cell.

C. Fabrication and measurement

To validate the proposed theory, an antenna prototype was fabricated and assembled. A multi-

channel programmable 0-30 V voltage controller based on Atmega128 processor and high voltage DACs is also designed and fabricated.

The radiation patterns for both vertically and horizontally polarization are measured and shown in Fig. 24. For 5-5 mode, the main lobe direction is 178°, 3 dB width is 77°. The gain of the COCO antenna is 3.6 dBi. The designed AFSS antenna is 7.0 dBi for 5-5 mode, 6.9 dBi for 4-6 mode and 6.6 dBi for 4-5-1 mode.

The configuration is shown in Fig. 25, and the measured results are shown in Fig. 26. The gains are directly shown in the figure for the reader to evaluate the energy distribution. Obviously, if there are more columns of the AFSS, it should be more flexible to control radiation, as well as with higher resolution.

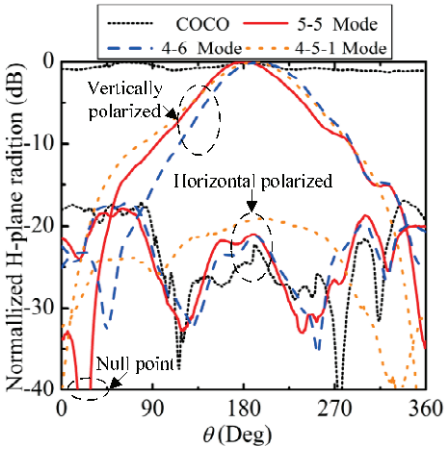

Fig. 24. Radiation patterns of single-beam modes and COCO antenna in H-plane.

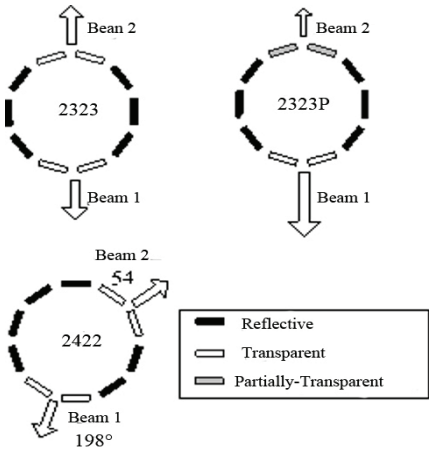

Fig. 25. Configuration methods of dual-beam modes.

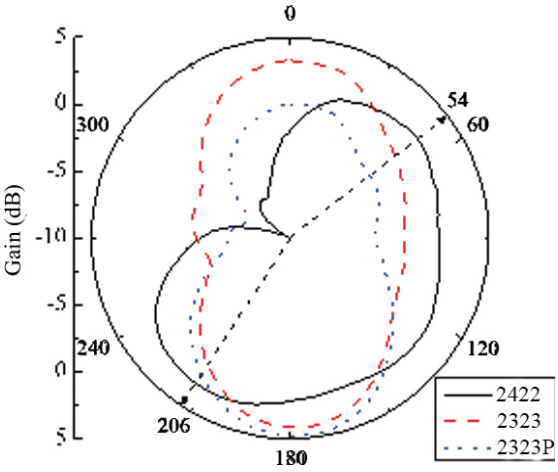

Fig. 26. Tested radiation patterns of the dual-beam modes in H-plane.

VII. CONCLUSION

The theory, design, simulation, measurement and application of metamaterials in the manipulations of electromagnetic waves have been discussed. First, the theory of transform optics is introduced briefly. Then electromagnetic concentrator and waveguide connector are proposed based on the transform optics. Both simulation and measurements results verify the theoretical results. Second, broadband polarization-insensitive absorber based on gradient structure metamaterial is designed and simulated. The metamaterial absorber has an excellent broadband property for its gradient structure. Simulation results verify that the designed sample has a good absorption effect on both TE wave and TM wave in a wide band. Third, a zero-index metamaterial is proposed for antenna gain enhancement. Both simulated and measured results show that the proposed metamaterial is able to achieve antenna gain enhancement in a broad frequency range from 8.9 GHz to 10.8 GHz and the greatest gain enhancement reaches up to 4.02 dB. Fourth, dual-polarity ultra-thin lens are proposed. The efficiency of cross-pol conversion approaches to the theoretical limit. The property of converging and diverging EM wave only depends on the helicity of the incident wave. Finally, a new AFSS structure mounted with varactor diodes has been proposed and designed. Then a radiation-pattern steerable antenna has been fabricated and tested based on the AFSS. By controlling the bias voltage, the radiation pattern sweeps in the whole

azimuth plane for both the single-beam modes and the dual-beam modes. In addition, the amplitudes of the two beams for dual-beam modes are also controllable. With sub-wavelength control of phase and amplitude of electromagnetic waves, we believe metamaterials will be a promising technology for the communication system of the next generation.

ACKNOWLEDGMENT

This work is supported by the National Natural Science Foundation of China (Grant No. 61371044, 61401122) and Ph.D. Programs Foundation of Ministry of Education of China (Grant No. 20122302120020).

REFERENCES

[1] V. G. Veselago, "The electrodynamics of substances with simultaneously negative values of ε and μ," *Sov. Phys. Uspekhi*, 10, pp. 509-514, 1968.

[2] J. B. Pendry, A. J. Holden, W. J. Stewart, and I. Youngs, "Extremely low frequency plasmons in metallic mesostructures," *Phys. Rev. Lett*., 76, pp. 4773-4776, 1996.

[3] J. B. Pendry, A. J. Holden, D. J. Robbins, and W. J. Stewart, "Magnetism from conductors and enhanced nonlinear phenomena," *IEEE Trans. Microwave Theory Tech*., 47, pp. 2075-2084, 1999.

[4] S. Enoch, G. Tayeb, P. Sabouroux, N. Guérin, and P. Vincent, "A metamaterial for directive emission," *Phys. Rev. Lett*., 89, pp. 213902-4, 2002.

[5] D. Schurig, J. J. Mock, B. J. Justice, S. A. Cummer, and J. B. Pendry, "Metamaterial electromagnetic cloak at microwave frequencies," *Science*, 314, 977-980, 2006.

[6] J. B. Pendry, "Negative refraction makes a perfect lens," *Phys. Rev. Lett*., 85, pp. 3966-3969, 2000.

[7] K. Zhang, F. Meng, Q. Wu, J. H. Fu, and L. W Li, "Waveguide connector constructed by normal layered dielectric materials based on embedded optical transformation," *EPL*, 99, pp. 47008-5, 2012.

[8] H. F. Ma and T. J. Cui, "Three-dimensional broadband and broad-angle transformation-optics lens," *Nat. Commun*., 1, pp. 124, 2010.

[9] T. Driscoll, G. Lipworth, J. Hunt, N. Landy, N. Kundtz, D. N. Basov, and D. R. Smith, "Performance of a three dimensional transformation-optical-flattened Lüneburg lens," *Opt. Express*, 20, pp. 13262-13273, 2012.

[10] L. Cong, W. Cao, Z. Tian1, J. Gu, J. Han, and W. Zhang, "Manipulating polarization states of terahertz radiation using metamaterials," *New J. Phys*., 14, pp. 115013, 2012.

[11] K. Zhang, Q. Wu, J. Fu, and L. W. Li. "Cylindrical electromagnetic concentrator with only axial constitutive parameter spatially variant," *J. Opt. Soc. Am. B*, 28, pp. 1573-1577, 2011.

[12] R. W. Ziolkowski, "Extraction of effective metamaterial parameters by parameter fitting of dispersive models," *IEEE Trans. Antennas Propag*., 51, pp. 1516-1529, 2003.

[13] E. Ekmekci and G. Turhan-Sayan, "Comparative investigation of resonance characteristics and electrical size of the double-sided SRR, BC-SRR and conventional SRR type metamaterials for varying substrate parameters," *PIER B*, 12, pp. 35-62, 2009.

[14] F. Y. Meng, Y. L. Li, K. Zhang, Q. Wu, and J. L. W. Li, "A detached zero index metamaterial lens for antenna gain enhancement," *PIER*, 132, pp. 463-478, 2012

[15] N. Yu, P. Genevet, M. A. Kats, F. Aieta, J. P. Tetienne, F. Capasso, and Z. Gaburro, "Light propagation with phase discontinuities: generalized laws of reflection and refraction," *Science*, 334, pp. 333-337, 2011.

[16] X. J. Ni, N. K. Emani, A. V. Kildishev, A. Boltasseva, and V. M. Shalaev, "Broadband light bending with plasmonic nanoantennas," *Science*, 335, pp. 427, 2012.

[17] F. Monticone, N. M. Estakhri, and A. Alù, "Full control of nanoscale optical transmission with a composite metascreen," *Phys. Rev. Lett*., 110, pp. 203903-5, 2013.

Qun Wu received his B.Sc. in Radio Engineering, his M. Eng. in Electromagnetic Fields and Microwaves, and his Ph.D. in Communication and Information Systems, all at Harbin Institute of Technology (HIT), Harbin, China in 1977, 1988, and 1999, respectively. He worked as a Visiting Professor at Seoul National University (SNU) in Korea, from 1998 to 1999, and Pohang University of Science and Technology, from 1999 to 2000, and a two-month short period of Visiting Professor at National University of Singapore from 2003 to 2010 and Nanyang Technological University in 2011, respectively. Since 1990, he has been with the School of Electronics and Information Engineering at HIT, China, where he is currently a Professor and a Director of Center for Microwaves and EMC.

Wu has published over 100 international and regional refereed journal papers. He is a Member of Microwave Society of the Chinese Institute of Electronics, and Senior Member of the IEEE. He is a Technical Reviewer for several international journals. His recent research interests are mainly in electromagnetic compatibility, metamaterals, RF microwave active and passive circuits, and millimeter wave MEMS devices. He is also a Vice Chair for IEEE Harbin Section, and Chair of IEEE Harbin EMC/AP/MTT Joint Society Chapter. He worked as a Chair or Member in the TPC of international conferences for many times. He also is invited to give a keynote report or invited papers in some international conferences for many times.

Kuang Zhang received the B.Eng. degree in Communication Engineering, the M.Eng. degree in Electronic Engineering and Ph.D. degree in Information and Communication Engineering, all from Harbin Institute of Technology, Harbin, China, in 2005, 2007 and 2011, respectively. Now he is the Assistant Professor with the School of Electronics and Information Engineering, HIT. His recent research interests are mainly in transform optics and ultra-thin metasurface.

Guohui Yang received the B.Eng. degree in Communication Engineering, the M.Eng. degree in Instrument Science and Engineering and Ph.D. degree in Microelectronics and Solid State Electronics, all from Harbin Institute of Technology, Harbin, China, in 2003, 2006 and 2009, respectively. Now he is the Assistant Professor and the Postdoctoral Fellow with the School of Electronics and Information Engineering, HIT. His recent research interests are mainly in frequency selective surface, tunable antenna; frequency selective surfaces; electromagnetic wave absorber.